Solid State Nuclear Magnetic Resonance 140 (2025) 102046

Contents lists available at ScienceDirect

Solid State Nuclear Magnetic Resonance

journal homepage: www.elsevier.com/locate/ssnmr

In-situ solid-state NMR spectroscopy reveals competing crystallization pathways for a system that forms structurally diverse multicomponent crystalline phases

Rose Gauttier, Colan E. Hughes, Benson M. Kariuki, Kenneth D.M. Harris *

School of Chemistry, Cardiff University, Park Place, Cardiff, Wales, CF10 3AT, UK

ARTICLE INFO

Handling Editor: Prof D Bryce

ABSTRACT

The development of NMR strategies for *in-situ* monitoring of crystallization processes has opened the opportunity to establish new mechanistic insights, including to understand the structural evolution of the solid phase produced in crystallization systems as a function of time. In this paper, we report the results of an *in-situ* solid-state ^{13}C NMR study of crystallization from a solution containing 1,10-dihydroxydecane and urea in methanol, leading to the identification of two structurally diverse multicomponent crystalline phases that are formed at different stages of the crystallization process. The initially produced phase is a urea inclusion compound, in which 1,10-dihydroxydecane guest molecules are included within the well-known urea host tunnel structure. Subsequently, a second crystalline phase is formed, which is identified as a stoichiometric hydrogen-bonded co-crystal 1,10-dihydroxydecane-(urea)$_2$. The *in-situ* solid-state ^{13}C NMR results suggest that the urea inclusion compound is not an intermediate phase on the crystallization pathway to form the co-crystal, as the urea inclusion compound remains after the formation of the co-crystal phase. However, after the appearance of the co-crystal phase, the subsequent crystallization process is dominated by rapid growth of the co-crystal rather than growth of the urea inclusion compound. The results demonstrate the capability of *in-situ* solid-state NMR strategies to monitor the structural evolution of multicomponent solid phases during crystallization from solution.

1. Introduction

While crystallization is central to many biological, chemical and industrial processes [1–10], the quest to derive a detailed understanding of crystallization mechanisms is often a challenging endeavour. However, the development of new and increasingly powerful experimental methods for time-resolved *in-situ* monitoring of crystallization processes [11] has expanded the opportunities to gain insights into the specific sequence of events that occur on the pathway from an initial homogeneous solution phase to the final solid product phase obtained in the crystallization process. In this regard, an important mechanistic aspect is to understand details of the structural evolution of the solid phase through different solid forms (such as polymorphs, solvate phases, or other multicomponent materials) on the pathway towards the final crystallization product.

In recent years, solid-state NMR strategies have been developed [12,13] for direct *in-situ* monitoring of crystallization processes from solution, relying on the fact that different solid phases containing a given type of molecule (which may encompass crystalline and/or amorphous phases) can generally be distinguished by high-resolution solid-state NMR spectroscopy. An advantage of using NMR techniques in such *in-situ* studies (compared to other spectroscopic techniques and/or diffraction-based techniques) is that the measurement conditions may be set up to detect only the solid phase within the heterogeneous solid-liquid system that exists during crystallization from solution, allowing the evolution of different solid phases to be monitored as a function of time without interference from signals due to the solute and/or solvent molecules in the liquid phase. In the case of crystallization of organic materials from solution, high-resolution solid-state ^{13}C NMR spectra containing signals only from the solid phase can be recorded using the ^{1}H→^{13}C cross-polarization (CP) NMR technique [14], which has been exploited in several applications of *in-situ* solid-state ^{13}C NMR studies of the crystallization of organic materials [15–17].

Further developments of *in-situ* solid-state NMR methodology for

This article is part of a special issue entitled: Advancements in SSNMR published in Solid State Nuclear Magnetic Resonance.

* Corresponding author.
E-mail address: HarrisKDM@cardiff.ac.uk (K.D.M. Harris).

https://doi.org/10.1016/j.ssnmr.2025.102046
Received 5 July 2025; Received in revised form 31 August 2025; Accepted 8 September 2025
Available online 9 September 2025

studying crystallization processes include the CLASSIC NMR (Combined Liquid- And Solid-State *In-situ* Crystallization NMR) technique [18], which provides essentially simultaneous information on the complementary changes that occur in the solid and liquid phases as a function of time during crystallization processes [19–22] by alternate recording of two (or more) different types of NMR spectra that selectively detect the solid phase and the liquid phase, respectively. In certain cases, the evolution of both the solid and liquid phases during crystallization (and other materials formation processes) can be monitored instead by recording a single type of NMR spectrum in which signals due to both the solid phase and the liquid phases are present, and are distinguished on the basis of their isotropic chemical shifts [16,23]. Advances in other NMR strategies to study crystallization processes include an *ex-situ* solid-state NMR strategy [24–26] that exploits the sensitivity advantages [27–30] of DNP NMR, and a DNP-based technique [31,32] in which hyperpolarized suspensions are subjected to rapid crystallization, with the hyperpolarized nuclei incorporated into the rapidly formed crystalline phase.

Here we focus on the analysis of *in-situ* solid-state ^{13}C NMR data recorded by repeated measurement of ^{1}H→^{13}C CP NMR spectra as a function of time during crystallization of 1,10-dihydroxydecane [HO$(CH_2)_{10}$OH; denoted 1,10-DHD; Fig. 1] and ^{13}C-labelled (99 %) urea (denoted ^{13}C-urea; Fig. 1) from methanol. We note that a preliminary report of the data from this study was included as part of a previous publication [33] illustrating the application of *in-situ* solid-state NMR techniques to detect the evolution of the solid phase through different solid forms during crystallization processes. In particular, focusing on the evolution of the peak due to ^{13}C-urea, it was shown that an initial solid phase is formed in the early stages of the crystallization process; however, after a period of time, relatively abrupt spectral changes occur, indicating the formation of a new solid phase, which was identified as a known 1,10-DHD-$(urea)_2$ co-crystal phase. Importantly, the previous work did not lead to a definitive assignment of the identity of the initially formed solid phase.

In the present paper, we report the structural assignment of the solid phases that are present at each stage of the crystallization process, including a definitive structural assignment of the initially formed solid phase, and a more detailed assessment of the variation in the amount of each phase present as a function of time. Importantly, while the previous analysis focused on the evolution of the intense signal due to ^{13}C-labelled urea in the *in-situ* solid-state ^{13}C NMR spectra, detailed analysis of the substantially weaker peaks due to 1,10-DHD (at natural isotopic abundance) in the present work has proven crucial in determining the structural assignments, which have also been facilitated by recording solid-state ^{13}C NMR data for samples of possible candidate phases prepared independently. The results demonstrate the capability of *in-situ* solid-state NMR strategies to monitor the evolution of structurally diverse multicomponent solid phases produced during crystallization from solution.

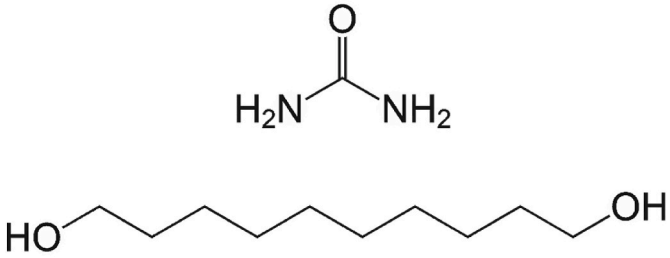

Fig. 1. Molecular structures of urea (top) and 1,10-dihydroxydecane (bottom).

2. Structural properties of potential solid products from the crystallization process

First, we discuss the crystalline phases that could potentially be formed in crystallization from a solution containing 1,10-DHD and urea in methanol, which include: (i) multicomponent crystalline phases containing both 1,10-DHD and urea (discussed in more detail below), (ii) the pure crystalline phase of urea [34–36], (iii) the pure crystalline phase of 1,10-DHD [37], and (iv) solvate phases containing 1,10-DHD and/or urea together with methanol. With regard to (iv), we note that no crystalline solvate structures containing urea and methanol or containing 1,10-DHD and methanol have been reported in the literature.

With regard to (i), urea is known to form different types of multicomponent crystalline phases with other molecules, in particular: (a) hydrogen-bonded co-crystals [38–51], in which urea and the other type of molecule are connected directly by intermolecular hydrogen bonding, and (b) urea inclusion compounds [52–60], in which guest molecules are located inside one-dimensional tunnels that exist within a urea host structure, which is constructed from a hydrogen-bonded network of urea molecules.

A hydrogen-bonded co-crystal containing 1,10-DHD and urea, with stoichiometry 1,10-DHD-$(urea)_2$, has been reported as part of a wider study [61,62] of the formation and structural properties of co-crystals containing urea and even-chain α,ω-dihydroxyalkanes [$HO(CH_2)_nOH$; $n = 2m$; $m = 3, 4 \ldots, 8$]. The crystal structures of these materials are based on stacking of hydrogen-bonded sheets; each sheet contains double-stranded hydrogen-bonded ribbons of urea molecules, which are linked through hydrogen bonding to the α,ω-dihydroxyalkane molecules, as shown for the 1,10-DHD-$(urea)_2$ co-crystal in Fig. 2a. The known crystal structures of these co-crystals are classified according to the type of hydrogen-bonded urea ribbon [which is either parallel (P) or anti-parallel (A-P)] and the geometric relationship between the urea ribbon and the axis of the α,ω-dihydroxyalkane molecule [which is either acute (A) or obtuse (O)]. Based on these features, the known 1,10-DHD-$(urea)_2$ co-crystal has the A-P/O structure type, which is also observed for co-crystals formed with longer α,ω-dihydroxyalkanes (n = 12, 14, 16). On the other hand, co-crystals with the A-P/A and P/A structure types have been observed for shorter α,ω-dihydroxyalkanes (with $n = 6$ and $n = 8$, respectively). We note that, while only the A-P/O structure type has so far been reported for the 1,10-DHD-$(urea)_2$ co-crystal, it is conceivable that polymorphs of the 1,10-DHD-$(urea)_2$ co-crystal based on the A-P/A or P/A structure types could be formed as intermediate phases on crystallization pathways to form the A-P/O structure type.

Urea inclusion compounds [52–60] are typically formed between urea and guest molecules that are based on long-chain *n*-alkanes or terminally functionalized *n*-alkanes [$X(CH_2)_nX$; for example, X = Cl, Br, I, CO_2H]. The structures of most urea inclusion compounds are characterized by the following features: (1) a hexagonal host tunnel structure at ambient temperature (Fig. 2b), which is constructed from a hydrogen-bonded network of urea molecules and contains a dense packing of guest molecules along each tunnel, (2) an incommensurate relationship [63,64] between the periodic repeat distances of the host and guest components along the tunnel direction, and (3) substantial dynamic disorder (reorientation about the tunnel axis) of the guest molecules at ambient temperature [65–69]. As a consequence of the incommensurate relationship between the host and guest components, these materials are generally non-stoichiometric and the urea:guest molar ratio is dictated by the periodic repeat distance of the guest molecules along the urea host tunnels. In the case of the urea inclusion compound containing 1,10-DHD guest molecules, the urea:guest molar ratio is *ca.* 9.56.

3. Results and discussion

For our *in-situ* solid-state ^{13}C NMR study of the crystallization of ^{13}C-

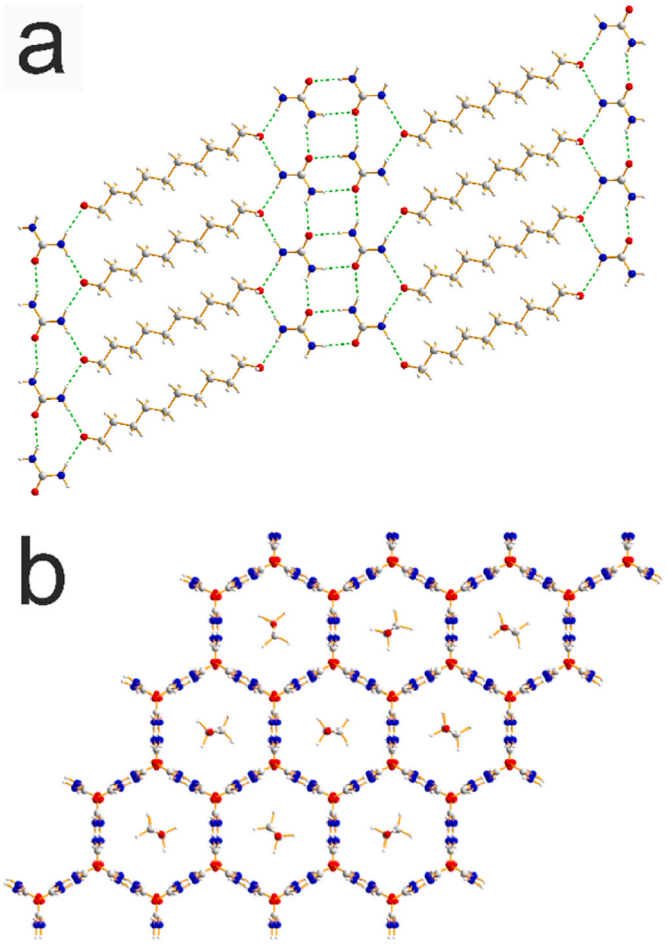

Fig. 2. Crystal structures of (a) the 1,10-DHD-(urea)$_2$ co-crystal with the A-P/O structure type (green dashed lines represent hydrogen-bonding interactions), and (b) the urea host tunnel structure in the 1,10-DHD/urea inclusion compound (the 1,10-DHD guest molecules have been inserted into the tunnels with random orientations around the tunnel axis, reflecting the orientational disorder that exists at ambient temperature). Colour scheme: C, grey; H, white; O, red; N, blue. (For interpretation of the references to colour in this figure legend, the reader is referred to the Web version of this article.)

labelled urea and 1,10-DHD from methanol, powder samples of ^{13}C-urea and 1,10-DHD (in 2:1 molar ratio) were mixed with methanol inside an NMR rotor at ambient temperature (see Section 5 for full details). The rotor was inserted into the solid-state NMR spectrometer, heated to 83 °C, and then maintained at this temperature for 3 h to ensure complete dissolution. To induce crystallization, the solution was cooled to 25 °C at a rate of 1.45 °C min^{-1} (total cooling time, 40 min). When the sample temperature reached 25 °C, the measurement of ^{1}H→^{13}C CP NMR spectra was started (which defines time = 0 in the *in-situ* NMR study of the crystallization process). Spectra were then measured repeatedly with the temperature kept constant at 25 °C for the total duration of the crystallization experiment (total time, 11.4 h; total number of spectra, 256; time per spectrum, 2.67 min). Crystallization of urea and 1,10-DHD under essentially the same conditions in a conventional laboratory set-up is known [61] to produce the 1,10-DHD-(urea)$_2$ co-crystal phase (with A-P/O structure type) as the final crystallization product. In contrast, to produce urea inclusion compounds under conventional laboratory crystallization conditions, the composition of the crystallization solution would typically be close to the expected urea: guest molar ratio in the inclusion compound (*ca.* 9.56 for the 1, 10-DHD/urea inclusion compound). Thus, the urea:1,10-DHD molar ratio of 2:1 used in our *in-situ* solid-state ^{13}C NMR study is significantly lower than the molar ratio that would typically be used for crystallization of the 1,10-DHD/urea inclusion compound.

To enhance the sensitivity of the *in-situ* solid-state ^{13}C NMR measurements, ^{13}C-labelled (99 %) urea was used, allowing high-quality spectra to be recorded in a short time (2.67 min), thus representing good time-resolution for the *in-situ* solid-state ^{13}C NMR study. As a consequence, however, the solid-state ^{13}C NMR spectra are dominated by signals from ^{13}C-urea, and the signal intensities due to 1,10-DHD (at natural isotopic abundances) are significantly lower, as discussed below.

All solid-state ^{13}C NMR spectra are referenced against the carboxylate ^{13}C environment (176.5 ppm) in the α polymorph of glycine [70]. For the present study, referencing of the *in-situ* solid-state ^{13}C NMR data was carried out independently of the referencing used in the previous work [33], including a more rigorous handling of the effects of the drift in magnetic field strength during the cooling process on the measured chemical shifts (the drift in magnetic field strength is due to cooling of the shim coils, which continued for a period of time after the sample temperature had reached 25 °C in the cooling process). As a consequence, the ^{13}C chemical shifts reported in the present paper are lower by *ca.* 0.2 ppm than those quoted previously [33].

An overview of the time-evolution of the solid phase during the crystallization process is obtained by considering the changes in the region of the solid-state ^{13}C NMR spectrum from 160 ppm to 170 ppm, which contains peaks due to ^{13}C-urea, as shown in Fig. 3 (see also Fig. S1a in Supporting Information). First, we note that no signal is observed in the *in-situ* solid-state ^{13}C NMR data (Figs. 3 and 4a,c) at the isotropic ^{13}C NMR chemical shift (162.65 ppm; Fig. 4f) characteristic of the pure crystalline phase of urea, indicating that this phase is not present at any stage of the crystallization process. The first spectrum recorded in the *in-situ* solid-state ^{13}C NMR study (after the temperature of the crystallization system reached 25 °C) contains a single isotropic peak for ^{13}C-urea at 163.9 ppm (we note that, as the intensity of this peak is already appreciable in the first spectrum, it is likely that the initial solid phase had already started to form before the end of the cooling process). As shown in Fig. 5, the intensity of this peak grows as a function of time before levelling off at *ca.* 40 min. At this time, a new peak appears suddenly at 164.4 ppm (Fig. 3), and grows rapidly during the next *ca.* 35 min (Fig. 5). The new peak significantly overlaps the peak due to the initial solid phase, such that the peak for the initial solid phase quickly becomes "hidden" beneath the peak from the new phase. However, close inspection suggests that the new peak is slightly asymmetric (see Fig. 6c), which is attributed to an unresolved contribution from the continued presence of the peak due to the initial solid phase. To confirm this assignment, the region containing peaks due to ^{13}C-urea in each spectrum recorded during the *in-situ* solid-state ^{13}C NMR study was fitted using Lorentzian lineshapes. For the spectra recorded up to *ca.* 40 min, a good fit to the experimental spectrum is obtained using a single Lorentzian peak at 163.9 ppm. However, for the spectra recorded after *ca.* 40 min, two Lorentzian peaks are required to obtain a good fit, with fitted values of isotropic ^{13}C NMR chemical shifts of 163.9 ppm and 164.4 ppm. Representative examples of peak fitting at different stages of the crystallization process are shown in Fig. 6, and the variation of the intensities of the two peaks (determined from the peak fitting) as a function of time during the crystallization process is shown in Fig. 7. We note that the measured intensities of these peaks are not necessarily indicative of the relative amounts of the initial phase and the new phase as the relative efficiencies of ^{1}H→^{13}C CP for these two phases under the measurement conditions used in our *in-situ* solid-state NMR study have not been calibrated [71]. After *ca.* 75 min, the total intensity of the ^{13}C-urea signal remains essentially constant [72] throughout the remaining period (*ca.* 10 hr) of the *in-situ* solid-state ^{13}C NMR study (Fig. 5), suggesting that the crystallization process had essentially reached completion by *ca.* 75 min. As discussed below, the new peak at 164.4 ppm that emerges at *ca.* 40 min corresponds to the known 1, 10-DHD-(urea)$_2$ co-crystal phase with the A-P/O structure type, which is the final product observed in laboratory crystallization experiments under essentially the same conditions.

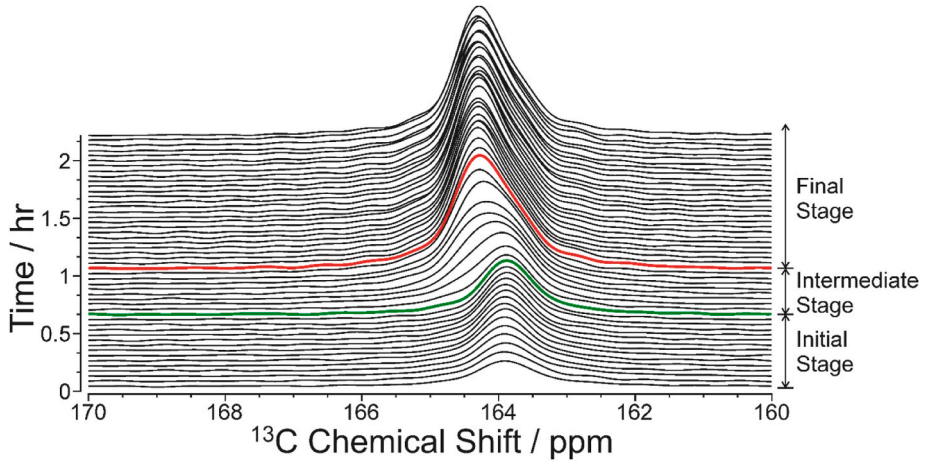

Fig. 3. Stack plot of the ^{1}H→^{13}C CP NMR spectra (showing the region from 160 ppm to 170 ppm corresponding to signals from ^{13}C-urea) recorded during the first 2.2 h of the *in-situ* solid-state ^{13}C NMR study. The periods of time corresponding to the initial, intermediate and final stages of the crystallization process are shown at the right; only the early part of the final stage (from 75 min to 2.2 h) is shown. The spectrum in green represents the end of the initial stage and the spectrum in red represents the end of the intermediate stage. (For interpretation of the references to colour in this figure legend, the reader is referred to the Web version of this article.)

From the observed evolution of the ^{13}C-urea peak as a function of time, as discussed above, it is convenient to describe the crystallization process in terms of three stages: (i) initial stage (the first 40 min), (ii) intermediate stage (from 40 min to 75 min), and (iii) final stage (from 75 min to the end of the experiment at 11.4 h).

We note that our previous discussion [33] of the *in-situ* solid-state ^{13}C NMR data focused on the evolution of the signals due to ^{13}C-urea as a function of time, which gave a broad overview of the changes in the solid phase during the crystallization process at the level discussed above. However, analysis of the ^{13}C-urea signals alone did not allow the structural identity of the initially produced solid phase to be determined, and furthermore, the changes in the amounts of the initial phase and the new phase as a function of time were not assessed. In the present work, we significantly extend our analysis of the *in-situ* solid-state ^{13}C NMR data, showing that analysis of the weak signals due to 1,10-DHD leads both to a definitive assignment of the solid phases present at each stage of the crystallization process and to an understanding of the evolution of the amounts of each solid phase present in the crystallization system as a function of time.

To facilitate the assignment of each solid phase present during the crystallization process, solid-state ^{13}C NMR spectra have been recorded for various solid phases (discussed in Section 2) that have the potential to be formed in crystallization from a solution containing urea and 1,10-DHD. Specifically, ^{1}H→^{13}C CP NMR spectra have been recorded for powder samples of the 1,10-DHD/urea inclusion compound (Fig. 4b), the known 1,10-DHD-(urea)$_2$ co-crystal phase [61] with A-P/O structure type (Fig. 4d), the pure crystalline phase of 1,10-DHD [37] (Fig. 4e), and the pure crystalline phase of urea [34–36] (Fig. 4f). From Fig. 4b, we note that the peaks due to 1,10-DHD in the solid-state ^{13}C NMR spectrum of the 1,10-DHD/urea inclusion compound are significantly sharper than those in the spectra for the other solid phases containing 1,10-DHD (Fig. 4d and e). Such narrow peaks are a characteristic feature for guest molecules in urea inclusion compounds as a consequence of rapid molecular dynamics (reorientation about the urea host tunnel axis), which has been studied previously [65–69] by solid-state NMR and other techniques.

We now focus on the peaks due to 1,10-DHD in the *in-situ* solid-state ^{13}C NMR spectra (in the region from 20 ppm to 70 ppm). These peaks have much lower intensities than those due to ^{13}C-urea, resulting in poor signal/noise in this region of each individual spectrum (see Fig. S1b). For this reason, we first consider the summation of all spectra recorded in the initial stage of the crystallization process (Fig. 4a), and the summation of all spectra recorded in the final stage of the crystallization process (Fig. 4c). These summed *in-situ* solid-state ^{13}C NMR spectra for the initial and final stages are now compared with the solid-state ^{13}C NMR spectra (Fig. 4b,d,e,f) recorded for powder samples of the solid phases that may potentially arise on the crystallization pathway.

From the summed *in-situ* solid-state ^{13}C NMR spectrum for the initial stage of the crystallization process (Fig. 4a), it is clear that the peak positions and the narrow peak widths are in excellent agreement with all the features of the solid-state ^{13}C NMR spectrum of the 1,10-DHD/urea inclusion compound (Fig. 4b). Furthermore, as no other peaks are observed in the summed *in-situ* solid-state ^{13}C NMR spectrum (Fig. 4a), we conclude that no other solid phase containing 1,10-DHD is present during the initial stage of the crystallization process. Our assignment from analysis of the peaks due to 1,10-DHD that the initial solid phase is the 1,10-DHD/urea inclusion compound is fully consistent with the peak observed for ^{13}C-urea at 163.9 ppm in the initial stage of the crystallization process (Figs. 3 and 4a), which is in close agreement with the isotropic ^{13}C NMR chemical shift (164.0 ppm) for ^{13}C-urea in the 1,10-DHD/urea inclusion compound (Fig. 4b).

From the summed *in-situ* solid-state ^{13}C NMR spectrum for the final stage of the crystallization process (Fig. 4c), it is clear that the peaks observed for the 1,10-DHD/urea inclusion compound in the initial stage (Fig. 4a) are still present in the final stage. However, new peaks due to 1,10-DHD are also observed in the final stage that were not present in the initial stage, and these new peaks are fully consistent with the solid-state ^{13}C NMR spectrum of the 1,10-DHD-(urea)$_2$ co-crystal phase (Fig. 4d). On this basis, we conclude that both the 1,10-DHD/urea inclusion compound and the 1,10-DHD-(urea)$_2$ co-crystal are present during the final stage of the crystallization process. These two multi-component solid phases account for all peaks observed in the region of the solid-state ^{13}C NMR spectrum (from 20 ppm to 70 ppm) corresponding to 1,10-DHD. A detailed rationalization of this conclusion is also shown in Fig. 8.

To explore whether any evolution occurs in the relative amounts of the 1,10-DHD/urea inclusion compound and the 1,10-DHD-(urea)$_2$ co-crystal phase as a function of time during the final stage of the crystallization process, we consider separate summations of the *in-situ* solid-state ^{13}C NMR spectra recorded in four different time periods during the final stage (Fig. S2), specifically from 75 min to 3.6 h, from 3.6 h to 6.2 h, from 6.2 h to 8.8 h, and from 8.8 h to 11.4 h. From the summed *in-situ* solid-state ^{13}C NMR spectrum for each time period, it is clear that no significant evolution of the solid phase occurs during the final stage, as the summed spectrum for each period contains the same peaks due to the 1,10-DHD/urea inclusion compound and the 1,10-DHD-(urea)$_2$ co-

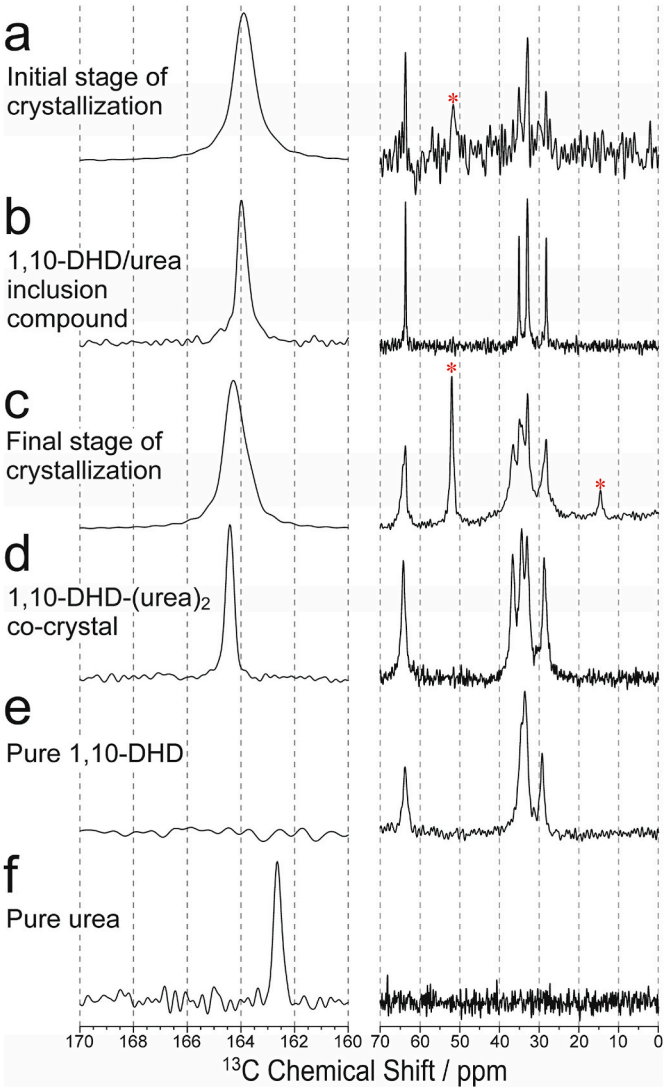

Fig. 4. (a) Summation of all the *in-situ* solid-state ^{13}C NMR spectra recorded in the initial stage (from 0 min to 40 min) of the crystallization process. (b) Solid-state ^{13}C NMR spectrum recorded for a powder sample of the 1,10-DHD/urea inclusion compound. (c) Summation of all the *in-situ* solid-state ^{13}C NMR spectra recorded in the final stage (from 75 min to 11.4 h) of the crystallization process. (d) Solid-state ^{13}C NMR spectrum recorded for a powder sample of the 1,10-DHD-(urea)$_2$ co-crystal with the A-P/O structure type. (e) Solid-state ^{13}C NMR spectrum recorded for a powder sample of the pure crystalline phase of 1,10-DHD. (f) Solid-state ^{13}C NMR spectrum recorded for a powder sample of the pure crystalline phase of urea. For (a) and (c), the samples contained ^{13}C-labelled urea; for (b), (d), (e) and (f), the samples contained urea at natural isotopic abundances. Spinning sidebands (from the ^{13}C-urea peak) are indicated by red asterisks.

crystal with the same relative intensities. While the relative amounts of the two solid phases cannot be quantified from these spectra (as the relative efficiencies of ^{1}H→^{13}C CP have not been calibrated), it is nevertheless clear that the relative amounts of the 1,10-DHD/urea inclusion compound and the 1,10-DHD-(urea)$_2$ co-crystal phase remain essentially constant during the final stage of the crystallization process.

4. Concluding remarks

The results from our *in-situ* solid-state ^{13}C NMR study of crystallization from a solution containing ^{13}C-urea and 1,10-DHD in methanol provide a clear demonstration that the formation and growth of two structurally diverse multicomponent crystalline phases, specifically the

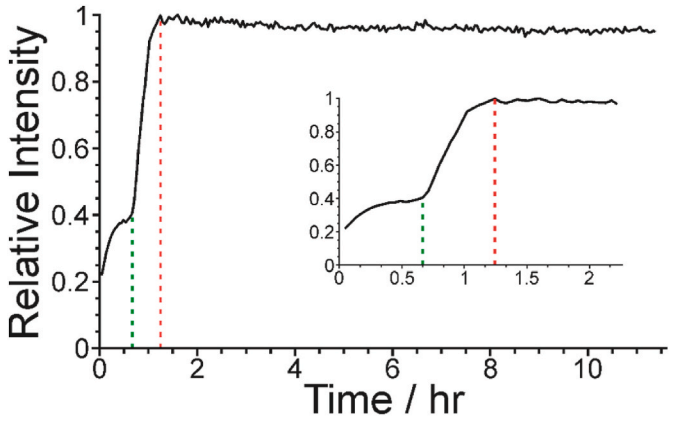

Fig. 5. Total intensity of the signals due to ^{13}C-urea as a function of time during the *in-situ* solid-state ^{13}C NMR study. The inset shows an expanded view of intensity *versus* time for the first 2.2 h of the crystallization process. The three stages of the crystallization experiment are identified as: (i) initial stage (the first 40 min; up to the green dashed line), (ii) intermediate stage (from 40 min to 75 min; between the green and red dashed lines), and (iii) final stage (from 75 min to 11.4 h; after the red dashed line). (For interpretation of the references to colour in this figure legend, the reader is referred to the Web version of this article.)

1,10-DHD/urea inclusion compound and the 1,10-DHD-(urea)$_2$ co-crystal with the A-P/O structure type, occurs at different stages of the crystallization process. Although the urea:1,10-DHD molar ratio in the initial crystallization solution is known (from conventional laboratory crystallization experiments) to lead to the 1,10-DHD-(urea)$_2$ co-crystal as the final crystallization product, there is a significant lag time (*ca.* 40 min) before the 1,10-DHD-(urea)$_2$ co-crystal phase is actually observed in the *in-situ* solid-state ^{13}C NMR study. In contrast, an amount of the 1,10-DHD/urea inclusion compound is already present in the crystallization system from the start of the *in-situ* solid-state ^{13}C NMR measurements, and grows during the first 40 min. These observations suggest that nucleation of the 1,10-DHD/urea inclusion compound is more facile than nucleation of the 1,10-DHD-(urea)$_2$ co-crystal phase under the conditions of the crystallization experiment. However, once nucleation of the 1,10-DHD-(urea)$_2$ co-crystal has occurred (at *ca.* 40 min), the subsequent crystallization process is dominated by growth of this phase, and no significant further growth of the 1,10-DHD/urea inclusion compound is observed once the 1,10-DHD-(urea)$_2$ co-crystal phase is present in the system.

Clearly, the preferential nucleation of the 1,10-DHD/urea inclusion compound alludes to the possibility that aggregation of the 1,10-DHD molecules and urea molecules in the pre-nucleation supersaturated solution (which exists prior to crystallization) occurs in a manner that favours nucleation of the 1,10-DHD/urea inclusion compound rather than nucleation of the 1,10-DHD-(urea)$_2$ co-crystal phase. In order to directly probe this issue, future studies will focus on applying the CLASSIC NMR strategy [18] to investigate the nature of the molecular aggregation in the liquid phase in the early (pre-nucleation) stages of the crystallization process, with the aim of understanding the reasons underlying the initial formation of the 1,10-DHD/urea inclusion compound, and to monitor the sequence of changes that occur in both the liquid and solid phases as a function of time during the subsequent stages of the crystallization process.

Finally, an interesting topic for future study will be to explore the spatial distribution of the two crystalline phases within the NMR rotor following *in-situ* NMR studies of the crystallization process reported here, recognizing that crystals of the initially produced solid phase (the 1,10-DHD/urea inclusion compound) and crystals of the subsequently produced solid phase [the 1,10-DHD-(urea)$_2$ co-crystal] may be localized in different regions of the rotor as a consequence of the effects of

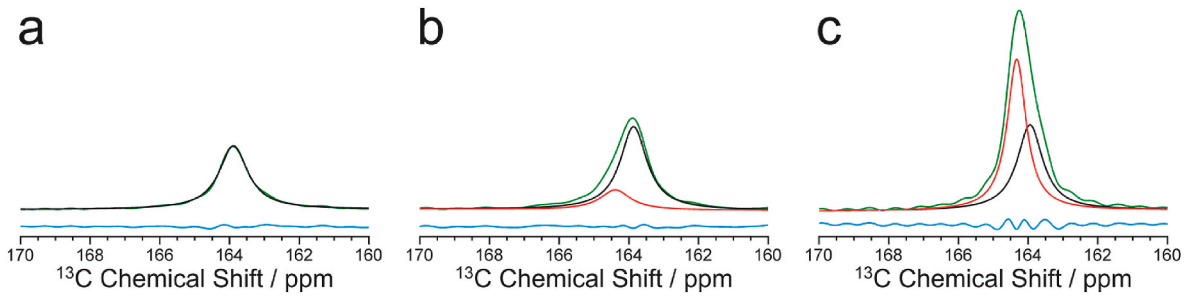

Fig. 6. Fitting of peaks due to ^{13}C-urea in the *in-situ* solid-state ^{13}C NMR data recorded during the crystallization process, based on one or two Lorentzian lineshapes. Specific fits are shown for the spectra recorded at: (a) 13 min (during the initial stage), (b) 45 min (near the start of the intermediate stage), and (c) 11.4 h (at the end of the final stage). Green – experimental spectrum; black – fitted peak at 163.9 ppm; red – fitted peak at 164.4 ppm; blue – difference between experimental and fitted peaks. (For interpretation of the references to colour in this figure legend, the reader is referred to the Web version of this article.)

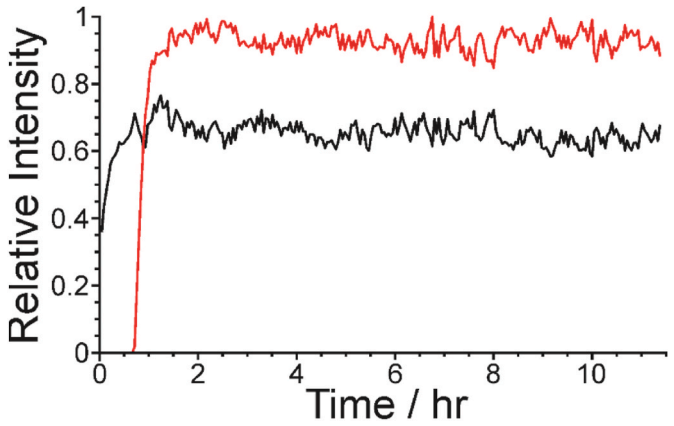

Fig. 7. Intensities of the peaks due to ^{13}C-urea in the 1,10-DHD/urea inclusion compound (black) and ^{13}C-urea in the 1,10-DHD-(urea)$_2$ co-crystal (red) determined by fitting the peaks due to ^{13}C-urea in the spectra recorded as a function of time during the *in-situ* solid-state ^{13}C NMR study. (For interpretation of the references to colour in this figure legend, the reader is referred to the Web version of this article.)

magic-angle sample spinning and the fact that the two phases are formed at different stages of the crystallization process.

5. Methods

All materials were purchased from Sigma-Aldrich. The *in-situ* solid-state ^{13}C NMR study was carried out on a Bruker AVANCE III NMR spectrometer (20.0 T; ^{13}C Larmor frequency, 213.8 MHz), which is the "850 MHz Instrument" at the U.K. High-Field Solid-State NMR Facility. To prepare the initial solution containing ^{13}C-labelled urea (99 %) and 1,10-DHD (at natural isotopic abundances) in methanol, powder samples of ^{13}C-urea (9.6 mg) and 1,10-DHD (13.9 mg) were mixed with methanol (16.0 mg) in a solid-state NMR rotor, corresponding to a urea:1,10-DHD molar ratio of 2:1. The NMR rotor was inserted into the solid-state NMR spectrometer, subjected to MAS at 8 kHz, heated to 83 °C, and then maintained at this temperature for 3 h to ensure complete dissolution. To induce crystallization, the sample in the NMR rotor was cooled to 25 °C at a rate of 1.45 °C min^{-1} (total cooling time, 40 min). When the sample temperature reached 25 °C, the measurement of ^{1}H→^{13}C CP NMR spectra was started, and was then continued repeatedly with the temperature kept constant at 25 °C for the total duration of the crystallization experiment (total time, 11.4 h).

The ^{1}H→^{13}C CP NMR spectra were recorded using ramped ^{1}H→^{13}C cross-polarization [73] with high-power ^{1}H decoupling using the SPINAL-64 technique [74] (MAS frequency, 8 kHz; CP contact time, 2.0 ms; decoupling nutation frequency, 71 kHz; recycle delay, 20 s; 8 scans

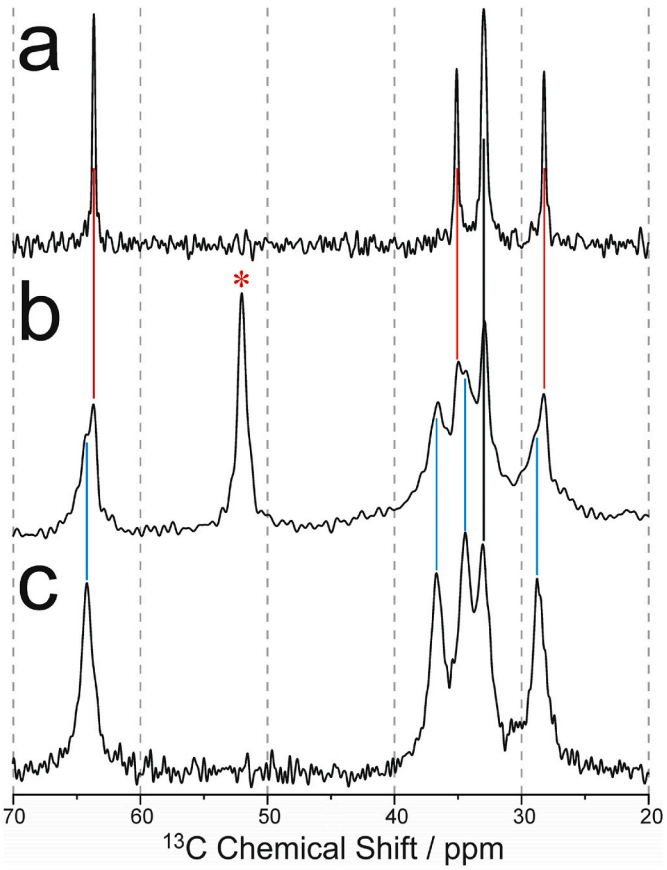

Fig. 8. Rationalization of the summation of all the *in-situ* solid-state ^{13}C NMR spectra recorded during the final stage (75 min to 11.4 h) of the *in-situ* solid-state ^{13}C NMR study [shown in (b) and in Fig. 4c] in terms of a contribution from the solid-state ^{13}C NMR spectrum characteristic of the 1,10-DHD/urea inclusion compound [shown in (a) and in Fig. 4b] and a contribution from the solid-state ^{13}C NMR spectrum characteristic of the 1,10-DHD-(urea)$_2$ co-crystal with the A-P/O structure type [shown in (c) and in Fig. 4d]. Red lines identify peaks due to the 1,10-DHD/urea inclusion compound, blue lines identify peaks due to the 1,10-DHD-(urea)$_2$ co-crystal, and the black line identifies a peak with contributions from both the 1,10-DHD/urea inclusion compound and the 1,10-DHD-(urea)$_2$ co-crystal. The peak marked by a red asterisk is a spinning sideband. (For interpretation of the references to colour in this figure legend, the reader is referred to the Web version of this article.)

acquired per spectrum preceded by 2 dummy scans). The method for temperature calibration was based on the ^{207}Pb NMR spectrum of lead nitrate [75,76], verified by measuring the ^{1}H NMR chemical shift difference between the two ^{1}H resonances of methanol [77–79]. More

details of the method for temperature calibration (including the method to account for the heating effects due to MAS) have been described previously [22].

Solid-state ^{13}C NMR spectra for powder samples of the 1,10-DHD/urea inclusion compound and the pure phase of 1,10-DHD were recorded on a Bruker AVANCE III HD NMR spectrometer (9.4 T; ^{13}C Larmor frequency, 100.64 MHz). Solid-state ^{13}C NMR spectra for powder samples of the 1,10-DHD-(urea)$_2$ co-crystal phase with the A-P/O structure type and the pure phase of urea were recorded on a Bruker AVANCE NEO NMR spectrometer (23.5 T; ^{13}C Larmor frequency, 251.57 MHz), which is the "1 GHz Instrument" at the U.K. High-Field Solid-State NMR Facility. Powder XRD data confirmed that the samples of the pure phase of 1,10-DHD, the pure phase of urea and the 1,10-DHD-(urea)$_2$ co-crystal phase (with the A-P/O structure type) were monophasic, while the sample of the 1,10-DHD/urea inclusion compound also contained a small amount of the pure phase of urea (the amount of this phase was insufficient to give a detectable signal under the conditions of the ^{1}H→^{13}C CP NMR measurement shown in Fig. 4b).

For all solid-state ^{13}C NMR spectra recorded during the *in-situ* solid-state ^{13}C NMR study, the region of the spectrum containing peaks due to ^{13}C-urea was fitted using Lorentzian lineshapes. Good quality fits (Fig. 6) were obtained using a single Lorentzian lineshape for the initial stage, and using two Lorentzian lineshapes for the intermediate and final stages of the crystallization process. For each Lorentzian lineshape, the intensity, chemical shift and linewidth were varied in the fitting process. In addition, for each spectrum, two parameters defining a linear baseline were also varied in the fitting process. Thus, the total number of fitted parameters per spectrum was five parameters for the initial stage, and eight parameters for the intermediate and final stages.

Declaration of competing interest

The authors declare that they have no known competing financial interests or personal relationships that could have appeared to influence the work reported in this paper.

Acknowledgements

We are grateful to the U.K. High-Field Solid-State NMR Facility for the allocation of spectrometer time for the *in-situ* solid-state ^{13}C NMR study, and to Dr Dinu Iuga (Facility Manager) for collaborative assistance with these experiments. The U.K. High-Field Solid-State NMR Facility was funded by EPSRC and BBSRC (EP/T015063/1 and, for the 1 GHz instrument, EP/R029946/1), as well as the University of Warwick, including part funding through Birmingham Science City Advanced Materials Projects 1 and 2 supported by Advantage West Midlands and the European Regional Development Fund. We are also grateful to Célina Cuennet (Cardiff University) for preparing the material used to record the spectrum in Fig. 4d, and to Cardiff University for support.

Appendix A. Supplementary data

Supplementary data to this article can be found online at https://doi.org/10.1016/j.ssnmr.2025.102046.

Data availability

Additional supporting experimental data for this article may be accessed at: https://doi.org/10.17035/cardiff.30099778

References

[1] M. Niederberger, H. Cölfen, Phys. Chem. Chem. Phys. 8 (2006) 3271–3287.
[2] F.C. Meldrum, H. Cölfen, Chem. Rev. 108 (2008) 4332–4432.
[3] L. Addadi, S. Weiner, Phys. Scripta 89 (2014) 098003.
[4] J.J. De Yoreo, P.U.P.A. Gilbert, N.A.J.M. Sommerdijk, R.L. Penn, S. Whitelam, D. Joester, H. Zhang, J.D. Rimer, A. Navrotsky, J.F. Banfield, A.F. Wallace, F. M. Michel, F.C. Meldrum, H. Cölfen, P.M. Dove, Science 349 (2015) aaa6760.
[5] X. Ye, M.R. Jones, L.B. Frechette, Q. Chen, A.S. Powers, P. Ercius, G. Dunn, G. M. Rotskoff, S.C. Nguyen, V.P. Adiga, A. Zettl, E. Rabani, P.L. Geissler, A. P. Alivisatos, Science 354 (2016) 874–877.
[6] A.G. Shtukenberg, M.D. Ward, B. Kahr, Chem. Rev. 117 (2017) 14042–14090.
[7] M.J.V. Vleet, T. Weng, X. Li, J.R. Schmidt, Chem. Rev. 118 (2018) 3681–3721.
[8] F.C. Meldrum, C. O'Shaughnessy, Adv. Mater. 32 (2020) 2001068.
[9] N. Fellah, I.J.C. Dela Cruz, B.G. Alamani, A.G. Shtukenberg, A.V. Pandit, M. D. Ward, A.S. Myerson, Cryst. Growth Des. 24 (2024) 3527–3558.
[10] S.S. Indri, F.M. Dietrich, A. Wagner, M. Hartstein, E. Nativ-Roth, M.J. Pavan, L. Kronik, M. Salvalaglio, B.A. Palmer, J. Am. Chem. Soc. 147 (2025) 19139–19147.
[11] N. Pienack, W. Bensch, Angew. Chem. Int. Ed. 50 (2011) 2014–2034.
[12] C.E. Hughes, K.D.M. Harris, J. Phys. Chem. A 112 (2008) 6808–6810.
[13] C.E. Hughes, K.D.M. Harris, Chem. Commun. 46 (2010) 4982–4984.
[14] S.R. Hartmann, E.L. Hahn, Phys. Rev. 128 (1962) 2042–2053.
[15] K.D.M. Harris, C.E. Hughes, P.A. Williams, Solid State Nucl. Magn. Reson. 65 (2015) 107–113.
[16] C.E. Hughes, P.A. Williams, V.L. Keast, V.G. Charalampopoulos, G.R. Edwards-Gau, K.D.M. Harris, Faraday Discuss. 179 (2015) 115–140.
[17] K.D.M. Harris, C.E. Hughes, P.A. Williams, G.R. Edwards-Gau, Acta Crystallogr., Sect. C: Struct. Chem. 73 (2017) 137–148.
[18] C.E. Hughes, P.A. Williams, K.D.M. Harris, Angew. Chem. Int. Ed. 53 (2014) 8939–8943.
[19] C.E. Hughes, P.A. Williams, B.M. Kariuki, K.D.M. Harris, ChemPhysChem 19 (2018) 3341–3345.
[20] C.E. Hughes, B. Walkley, L.J. Gardner, S.A. Walling, S.A. Bernal, D. Iuga, J. L. Provis, K.D.M. Harris, Solid State Nucl. Magn. Reson. 99 (2019) 1–6.
[21] C.L. Jones, C.E. Hughes, H.H.-M. Yeung, A. Paul, K.D.M. Harris, T.L. Easun, Chem. Sci. 12 (2021) 1486–1494.
[22] C.E. Hughes, N.V. Ratnasingam, P.A. Williams, E. Benhenou, R. Patterson, K.D. M. Harris, Faraday Discuss 255 (2025) 520–552.
[23] N.L. Kelly, E.A.L. Borthwick, G.B. Lawrence, P.S. Wheatley, C.E. Hughes, K.D. M. Harris, R.E. Morris, S.E. Ashbrook, Chem. Sci. 16 (2025) 4245–4255.
[24] P.C. Vioglio, P. Thureau, M. Juramy, F. Ziarelli, S. Viel, P.A. Williams, C.E. Hughes, K.D.M. Harris, G. Mollica, J. Phys. Chem. Lett. 10 (2019) 1505–1510.
[25] M. Juramy, R. Chèvre, P.C. Vioglio, F. Ziarelli, E. Besson, S. Gastaldi, S. Viel, P. Thureau, K.D.M. Harris, G. Mollica, J. Am. Chem. Soc. 143 (2021) 6095–6103.
[26] M. Juramy, P.C. Vioglio, F. Ziarelli, S. Viel, P. Thureau, G. Mollica, Solid State Nucl. Magn. Reson. 122 (2022) 101836.
[27] Q.Z. Ni, E. Daviso, T.V. Can, E. Markhasin, S.K. Jawla, T.M. Swager, R.J. Temkin, J. Herzfeld, R.G. Griffin, Acc. Chem. Res. 9 (2013) 1933–1941.
[28] A.J. Rossini, A. Zagdoun, M. Lelli, A. Lesage, C. Copéret, L. Emsley, Acc. Chem. Res. 46 (2013) 1942–1951.
[29] L. Zhao, A.C. Pinon, L. Emsley, A.J. Rossini, Magn. Reson. Chem. 56 (2017) 583–609.
[30] I.B. Moroz, M. Leskes, Annu. Rev. Mater. Res. 52 (2022) 25–55.
[31] E.M.M. Weber, T. Kress, D. Abergel, S. Sewsurn, T. Azaïs, D. Kurzbach, Anal. Chem. 92 (2020) 7666–7673.
[32] E. Turhan, C. Pötzl, W. Keil, M. Negroni, K. Kouřil, B. Meier, J.A. Romero, K. Kazimierczuk, I. Goldberga, T. Azaïs, D. Kurzbach, J. Phys. Chem. C 127 (2023) 19591–19598.
[33] C.E. Hughes, P.A. Williams, T.R. Peskett, K.D.M. Harris, J. Phys. Chem. Lett. 3 (2012) 3176–3181.
[34] R.W.G. Wyckoff, R.B. Corey, Z. Kristallogr. 89 (1934) 462–468.
[35] P. Vaughan, J. Donohue, Acta Crystallogr. 5 (1952) 530–535.
[36] A. Caron, J. Donohue, Acta Crystallogr. Sect. B Struct. Crystallogr. Cryst. Chem. 25 (1969) 404.
[37] N. Nakamura, T. Sato, Acta Crystallogr., Sect. C: Cryst. Struct. Commun. 55 (1999) 1685–1687.
[38] S. Harkema, J.H.M. ter Brake, R.B. Helmholdt, Acta Crystallogr., Sect. C: Cryst. Struct. Commun. 40 (1984) 1733–1734.
[39] J. Emsley, N.M. Reza, R. Kuroda, J. Crystallogr, Spectrosc. Res. 16 (1986) 57–69.
[40] H. Wiedenfeld, F. Knoch, Acta Crystallogr., Sect. C: Cryst. Struct. Commun. 46 (1990) 1038–1040.
[41] M.D. Hollingsworth, B.D. Santarsiero, H. Oumar-Mahamat, C.J. Nichols, Chem. Mater. 3 (1991) 23–25.
[42] M.D. Hollingsworth, M.E. Brown, B.D. Santarsiero, J.C. Huffman, C.R. Goss, Chem. Mater. 6 (1994) 1227–1244.
[43] V. Videnova-Adrabińska, M.C. Etter, J. Chem. Crystallogr. 25 (1995) 823–829.
[44] G. Smith, K.E. Baldry, K.A. Byriel, C.H.L. Kennard, Aust. J. Chem. 50 (1997) 727–736.
[45] G. Smith, K.E. Baldry, C.H.L. Kennard, K.A. Byriel, Aust. J. Chem. 50 (1997) 737–740.
[46] G. Smith, C.H.L. Kennard, K.A. Byriel, Aust. J. Chem. 50 (1997) 1021–1026.
[47] A.E. Aliev, K.D.M. Harris, P.H. Champkin, J. Phys. Chem. B 109 (2005) 23342–23350.
[48] S.-O. Lee, B.M. Kariuki, K.D.M. Harris, New J. Chem. 29 (2005) 1266–1271.
[49] A.J. Cruz-Cabeza, G.M. Day, W. Jones, Chem. Eur J. 14 (2008) 8830–8836.
[50] Z. Deutsch, J. Bernstein, Cryst. Growth Des. 8 (2008) 3537–3542.
[51] K. Chadwick, R. Davey, G. Sadiq, W. Cross, R. Pritchard, CrystEngComm 11 (2009) 412–414.
[52] A.E. Smith, Acta Crystallogr. 5 (1952) 224–235.
[53] K.D.M. Harris, J.M. Thomas, J. Chem. Soc., Faraday Trans. 86 (1990) 2985–2996.

[54] K.D.M. Harris, M.D. Hollingsworth, Proc. R. Soc. London, Ser. A 431 (1990) 245–269.
[55] D. Schmicker, S. van Smaalen, J.L. de Boer, C. Haas, K.D.M. Harris, Phys. Rev. Lett. 74 (1995) 734–737.
[56] M.D. Hollingsworth, M.E. Brown, A.C. Hillier, B.D. Santarsiero, J.D. Chaney, Science 273 (1996) 1355–1359.
[57] F. Guillaume, J. Chim. Phys. (Paris) 96 (1999) 1295–1315.
[58] M.D. Hollingsworth, Science 295 (2002) 2410–2413.
[59] J. Marti-Rujas, A. Desmedt, K.D.M. Harris, F. Guillaume, J. Am. Chem. Soc. 126 (2004) 11124–11125.
[60] K.D.M. Harris, Supramol. Chem. 19 (2007) 47–53.
[61] J. Martí-Rujas, B.M. Kariuki, C.E. Hughes, A. Morte-Ródenas, F. Guo, Z. Glavcheva-Laleva, K. Taştemür, L.-L. Ooi, L. Yeo, K.D.M. Harris, New J. Chem. 35 (2011) 1515–1521.
[62] Y. Zhou, F. Guo, C.E. Hughes, D.L. Browne, T.R. Peskett, K.D.M. Harris, Cryst. Growth Des. 15 (2015) 2901–2907.
[63] A.J.O. Rennie, K.D.M. Harris, Proc. R. Soc. London, Ser. A 430 (1990) 615–640.
[64] S. van Smaalen, K.D.M. Harris, Proc. R. Soc. London, Ser. A 452 (1996) 677–700.
[65] M.S. Greenfield, R.L. Vold, R.R. Vold, Mol. Phys. 66 (1989) 269–298.
[66] K.D.M. Harris, P. Jonsen, Chem. Phys. Lett. 154 (1989) 593–598.
[67] F. Guillaume, C. Sourisseau, A.J. Dianoux, J. Chem. Phys. 93 (1990) 3536–3541.
[68] A.E. Aliev, S.P. Smart, K.D.M. Harris, J. Mater. Chem. 4 (1994) 35–39.
[69] P. Girard, A.E. Aliev, F. Guillaume, K.D.M. Harris, M.D. Hollingsworth, A.-J. Dianoux, P. Jonsen, J. Chem. Phys. 109 (1998) 4078–4089.
[70] R.E. Taylor, Concepts Magn. Reson. 22A (2004) 79–89.
[71] We note that, for a given value of CP contact time used to measure the $^{1}H\rightarrow^{13}C$ CP NMR spectrum, the relative signal intensities for the two phases depend on the rate of $^{1}H\rightarrow^{13}C$ polarization transfer and the values of $T_{1\rho}(^{1}H)$ and $T_{1\rho}(^{13}C)$ for each phase. Furthermore, the relative signal intensities depend on the values of $T_1(^{1}H)$ for each phase relative to the recycle delay used to measure the $^{1}H\rightarrow^{13}C$ CP NMR spectrum.
[72] From Fig. 5, we note that there is a slight decrease (by a few percent) in the total signal intensity during the final stage of the crystallization process, which is most likely attributable to minor instrumental instabilities (e.g., gradual loss of optimization of the tuning of the probe) during the final ca. 10 hr of the experiment.
[73] G. Metz, X.L. Wu, S.O. Smith, J. Magn. Reson. A 110 (1994) 219–227.
[74] B.M. Fung, A.K. Khitrin, K. Ermolaev, J. Magn. Reson. 142 (2000) 97–101.
[75] A. Bielecki, D.P. Burum, J. Magn. Reson. A 116 (1995) 215–220.
[76] T.F. Kemp, G. Balakrishnan, K.J. Pike, M.E. Smith, R. Dupree, J. Magn. Reson. 204 (2010) 169–172.
[77] A.L. Van Geet, Anal. Chem. 40 (1968) 2227–2229.
[78] A.L. Van Geet, Anal. Chem. 42 (1970) 679–680.
[79] A.E. Aliev, K.D.M. Harris, Magn. Reson. Chem. 32 (1994) 366–369.